Adaptive Proxy-based Controller of an Active Ankle Foot Orthosis to Assist Lower Limb Movements of Paretic Patients

Journal:	*Robotica*
Manuscript ID	ROB-REG-18-0190
Manuscript Type:	Research Article
Date Submitted by the Author:	20-Jul-2018
Complete List of Authors:	Huo, Weiguang; Laboratory of Images, Signals and Intelligent Systems (LISSI) Arnez-Paniagua, Victor Ding, Guangzheng amirat, yacine; Images, Signals and Intelligent Systems Lab. LISSI-University of Paris 12, MOHAMMED, Samer; University of Paris Est Créteil,
Keywords:	Ankle foot orthosis, Adaptive PSMC, Wearable robot, Gait rehabilitation, Online reference generation

Submitted to the Special Issue on Wearable Robotics in the journal Robotica, Cambridge University Press 2018
doi:10.1017/S ...

ADAPTIVE PROXY-BASED CONTROLLER OF AN ACTIVE ANKLE FOOT ORTHOSIS TO ASSIST LOWER LIMB MOVEMENTS OF PARETIC PATIENTS

Weiguang Huo✉, Victor Arnez-Paniagua, Guangzheng Ding, Yacine Amirat and Samer Mohammed

Abstract

This paper deals with the control of an active ankle foot orthosis (AAFO) for paretic patients. State of the art methods using an AAFO try to track a pre-defined trajectory of the ankle joint while guaranteeing the wearer safety in the presence of a large tracking error. Combining the wearer's safety and tracking accuracy is generally difficult to achieve at the same time, hence a trade-off should be found. Proxy-based Sliding Mode Control (PSMC) offers great performances in tracking a desired trajectory while suffering from limited performances with respect to parameter uncertainties and external disturbances that generally occur during walking. This paper introduces an adaptation interaction method to the basic PSMC with an online adaptation of the proportional, integral and derivative gains. At the same time, a gait phase based ankle reference generation algorithm was proposed to adjust the joint reference trajectory in real time. The experiments using the AAFO shows better tracking results with respect to basic PSMC while guaranteeing the safety.

Keywords and phrases: Ankle foot orthosis, Online reference generation, Adaptive PSMC, Wearable robot, Gait rehabilitation

1. Introduction

Paretic patients generally present a limited movement of the ankle joint, which affects the quality of life of the patient. This reduced mobility are produced by pathologies at the ankle joint that can be divided based on the direction of the movement. For example, in the dorsiflexion direction, foot drop and foot slap are common described pathologies, the former is the inability to lift the tip of the foot during the swing phase of the gait, and the

✉Corresponding author.

later is an uncontrolled landing of the toes following the heel strike [1, 2]. In the plantar flexion direction, a common affliction is the reduced push off power of the toe to prepare the leg for the swing phase. Such gait pathologies slow down the walking speed and increase the fall risks.

Ankle foot orthoses (AFO) have been designed to correct the abnormal gait pattern and can generally be classified into three categories: passive, semi-active and active [3]. In the early stages of the gait rehabilitation, the patient normally presents less voluntary movement at the ankle joint, which results in a higher requirement for direct assistance. On the contrary, a patient that can produce sufficient ankle movement during walking could benefit more from a more compliant, semi-active device. For this reason, both active and semi-active orthosis are important in the integral rehabilitation process. In recent years, several active and semi-active ankle foot orthosis have been developed and different control strategies have been proposed to improve the benefits of active rehabilitation. Semi-active devices normally include an energy-storing element in the mechanical design to distribute the ankle joint energy in a desired pattern during the gait but are not able to introduce new sources of energy to assist the ankle joint. On the contrary, active ankle foot orthoses (AAFO) use direct actuation on the ankle joint. Examples of these devices are those that use series elastic actuators to produce the assistance torque [4, 5, 6, 7], use electro-hydraulic actuation for both plantar and dorsiflexion assistance [8, 9, 10, 11], or do not use energy-storing elements but use DC motors instead [12, 13].

The control strategies to determine the magnitude of the assistance provided by the orthoses can be classified in four groups [3, 6]: 1) orthoses that apply a pre-selected assistance torque with respect to the detected gait phase [6, 10, 14, 15], 2) devices that produce assistance as a function of electromyography (EMG) signals [9, 16], 3) those that adapt the stiffness, inertia or impedance of the orthetic device based on the detected gait phase, [4, 17, 18, 19], or 4) orthoses provide assistance torque as a function of the error between the current ankle joint angle and a reference trajectory pattern commonly generated from healthy walking profiles [5, 11, 20, 21, 22, 23, 24, 25, 26, 27]. It is important for the AAFO to produce a smooth, continuous and repeatable movement of the ankle joint in a clinical environment [28], as the control method used for each exoskeleton has a direct impact on the level and rate of human adaptation to the active device [29]. The control challenges of an AAFO are mainly related to: i) a high nonlinearity of the AAFO; ii) the human-robot transparency as the interaction dynamics between the human and the robot varies from one wearer to another, and iii) important uncertainties related to interaction with the wearer's voluntary movement and interaction with external environment. In addition to the foregoing, intrinsic safety is very important for any rehabilitation robot that has a close interaction with patients [30]. A large position error may

provoke a violent and thus unsafe response of the human-robot system and may cause physical damage to the wearer. Although there are various control methods that have been developed in the literature to control the AAFO, most of them are not able to guarantee both safety and high tracking accuracy. Sliding mode control (SMC) has gained much attention due to its design simplicity and robustness with respect to external disturbances [31]. However, the well known chattering side effect may excite high frequency dynamics of the system and may produce a large control output. Adaptive control based approaches are sufficiently robust with respect to uncertain disturbances, but the relative high controller gains may be harmful and risky for the wearer safety [32]. Proxy-based sliding mode control (PSMC), introduced in [33] efficiently combines the conventional SMC with PID control methods to increase the safety of the closed-loop system compared to the traditional PID control method. In other words, PSMC guarantees the safety when large tracking error occurs and ensures similar tracking performance during normal operation as that of the PID control. Since the AAFO system parameters and external disturbances vary from subject to subject, the fixed PID control gains in PSMC limit its tracking and robustness performances.

This paper proposes a new adaptive proxy based sliding mode control (APSMC) applied to the AAFO by introducing an adaptation interaction method [34], which allows online tuning of the PID gains in the PSMC scheme. Therefore, the proposed APSMC is able to adapt to the changes in the system's dynamics and external disturbances, while providing a better tracking performance with respect to standard PSMC. Furthermore, the benefit of safety is preserved. Furthermore, an on-line adaptive reference trajectory is proposed as a function of the walking speed of the wearer and the identification of the transitions between the different gait sub-phases. This adaptation of the reference trajectory avoids the use of a unique predefined trajectory of the ankle joint. It also allows the wearer focusing on the task and not on the synchonization with the reference trajectory.

The rest of this paper is organized as follows. Section 2 describes the human orthosis system. In Section 3, an online gait-phase based gait reference generation algorithm is presented using the ground reaction forces. In Section 4, the APSMC control method is proposed and its stability is analyzed. Moreover, an experimental validation of the proposed method with two healthy subjects and a paretic patient is presented in Section 5. Section 6 draws the conclusion of the study.

2. System Description

The orthosis used in this study is an actuated ankle foot orthosis (AAFO) attached to the subject's left leg, by means of straps to fix the robot to the

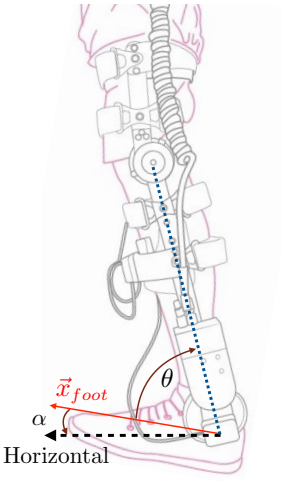

Figure 1: The angles determining the foot and the shank orientations.

calf and thigh, as shown in Figure 1. The orthosis has one active and one passive degrees of freedom (DoF), at the ankle and knee joint levels, respectively. The AAFO is considered as rigidly fixed to the subject's leg. The foot and the AAFO are considered as one unit referred to as the AAFO system. In this study, the problem of misalignment between the ankle joint and the AAFO's rotational axis when donning the device has been considerably reduced by adjusting manually the orthosis to every wearer's morphology using adaptable straps. Special cares have been taken during experiments in order to avoid reaching of the full ankle joint flexion/extension which considerably reduce the joint misalignment.

In order to model the AAFO system, denote by θ the angle between the foot and the shank and by α the angle between the foot and the horizontal axis (Figure 1). Only θ is measured using the embedded encoders in the AAFO.

The AAFO system's dynamics can be expressed as the sum of internal and external torques affecting the ankle joint as follows:

$$J\ddot{\theta} = \tau_f + \tau_a + \tau_s + \tau_r + \tau_g + \tau_h + \tau \tag{1}$$

where J is the moment of inertia of the foot, τ_f is the solid and viscous friction torques, τ_a is the torque induced by the translational acceleration of the foot, τ_s is the system's joint stiffness torque, τ_r is the torque induced by the ground reaction forces, τ_g is the gravity torque exerted by the foot on the ankle, τ_h is the torque produced by the plantar flexion and dorsiflexion muscle groups, and τ is the torque developed by the AAFO's actuator. All the torques are considered positive if they induce a counter clockwise

rotation. Furhtermore, the torques and their rate of change are considered bounded.

Each of the aforementioned torques is defined as follows:

$$\begin{aligned}\tau_f &= -k_{f_S}\text{sign}\dot{\theta} - k_{f_V}\dot{\theta}\\ \tau_a &= -k_a(a_y\cos\alpha - a_x\sin\alpha)\\ \tau_s &= -k_s(\theta-\theta_r)\\ \tau_r &= -k_r(x_gF_r)\cos\alpha\\ \tau_g &= -k_g\cos\alpha\end{aligned} \tag{2}$$

where, k_{f_S} and k_{f_V} are the solid and viscous friction coefficients, k_s is the system's stiffness coefficient, k_a is the system's acceleration torque coefficient, a_x and a_y are the horizontal and vertical linear accelerations, k_r is the ground reaction force coefficient, F_r is the equivalent GRF applied to the center of mass of the foot, x_g is the distance of the center of mass from the ankle joint, and $k_g = mgx_g$ is the system's gravity torque coefficient, where m and g, represent the mass of the foot and the gravity acceleration coefficient. Replacing (2) in (1) we obtain:

$$\begin{aligned}J\ddot{\theta} + k_{f_V}\dot{\theta} + k_s\theta = &-k_g\cos\alpha - k_{f_S}sign\dot{\theta} + k_s\theta_r\\ &-k_a(a_y\cos\alpha - a_x\sin\alpha)\\ &-k_r(x_gF_r)\cos\alpha + \tau_h + \tau\end{aligned} \tag{3}$$

The system internal and external torques are considered as disturbances to the system. Therefore, (3) can be rewritten as:

$$J\ddot{\theta} + B\dot{\theta} + K\theta = \tau + d, \tag{4}$$

with

$$\begin{aligned}d = &-k_g\cos\alpha - k_{f_S}sign\dot{\theta} + k_s\theta_r\\ &-k_a(a_y\cos\alpha - a_x\sin\alpha) - k_r(x_gF_r)\cos\alpha + \tau_h\end{aligned} \tag{5}$$

where $B = k_{f_V}$ and $K = k_s$. d represents all the non-linear disturbances.

3. On-line Reference Gait Generation

In order to control the AAFO system, a reference trajectory that represents the healthy ankle joint profile during the gait is required. To produce this reference, a motion capture system (Motion Analysis Corporation, Santa Rosa, CA, USA, six cameras, Sampling Frequency 100 Hz) and two force plates (AMTI, Watertown, MA, USA, Sampling Frequency 1000 Hz) were used to measure the normal gait of 20 healthy participants and calculate the average profile, for more details on this capture system please refer to [35]. However, it is important for the reference used for the controller

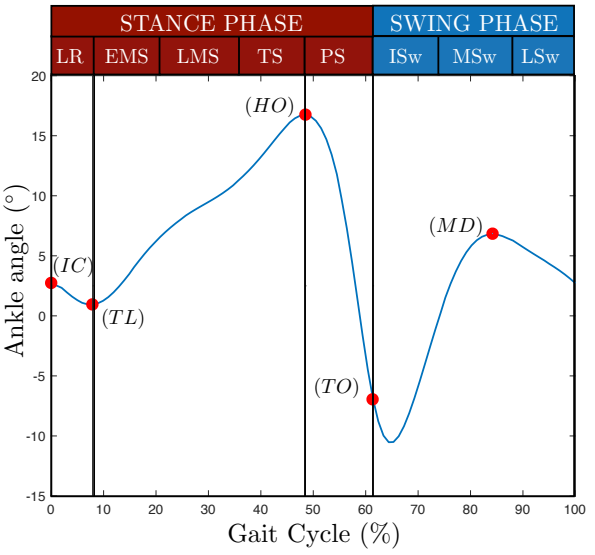

Figure 2: The healthy ankle joint angle profile normalized to the gait cycle. The gait cycle is divided in the sub-phases and the gait events are marked.

to be synchronized to the wearer's gait. For this purpose, two technics are mostly used; 1) to repeatedly generate the healthy ankle joint profile with a time-fixed periodicity, and use a audible or visual cue for the wearer to synchronize, or 2) to adapt in real-time the reference to the wearer's walking speed. For this study, an adaptive reference is considered and the method to generate it is described in the following.

3.1. Gait phases The gait cycle can be divided in stance and swing phases, as it is shown in Figure 2. To analyze the stance phase, it is further divided into sub-phases that are defined by the interaction of the feet with the ground, these are: loading response (LR), early-mid-stance (EMS), late-mid-stance (LMS), terminal stance (TS), pre-swing (PS). The swing phase is also divided based on the position of the foot relative to the oposite foot, these sub-phases are: initial swing (ISw), mid-swing (MSw), and terminal swing (TSw). Therefore, the transition between the stance sub-phases are triggered by specific events during the gait, such as initial contact (IC), toe landing (TL), heel off (HO), and toe off (TO). During the swing phase, the maximum dorsiflexion (MD) can be identified. Also, the gait event during the stance phase occur at the moments when the ankle joint angle profile switches from dorsiflexion to plantar-flexion and vice-versa as it is shown in Figure 2.

3.2. Gait phase detection In order to detect the gait events, a force sensitive resistor matrix (FSRM) embedded in each insole (Tekscan Co.) is

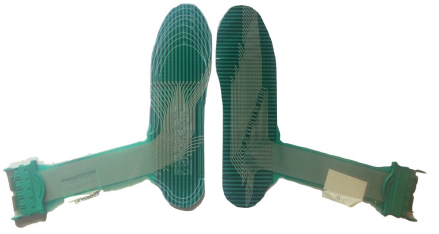

Figure 3: The Tekscan FSR insole

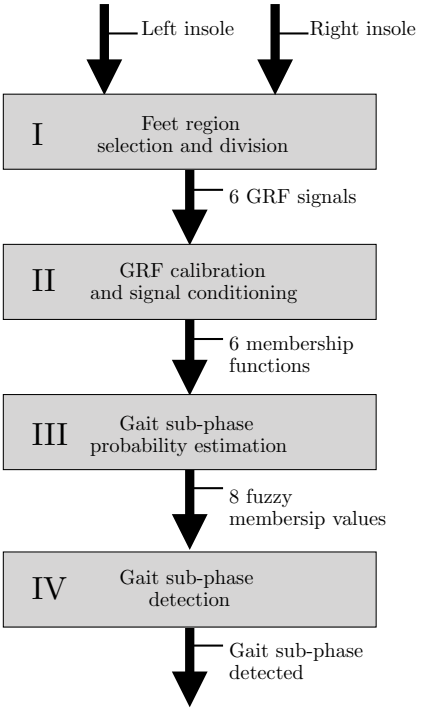

Figure 4: The algorithm to detect the gait sub-phases based on the signals from the insoles embedded with force sensitive resistor matrices.

used to measure the interaction between the feet and the ground, as shown in Figure 3. The algorithm to detect the gait sub-phases is described in four blocks, as shown in Figure 4, and are presented as follows. The measured surface of each insole is divided in three regions: the heel, the mid foot, and the toes areas. Then, the summatory of all the FSRM nodes for each region is calculated as described in block I.

In the block II, the six signals from the different areas of the feet are calibrated by detecting the minimum and maximum values from the begining of the session.

$$r_j = max(\vec{F}_{tj}) - min(\vec{F}_{tj}) \tag{6}$$

where r_j contains the range of the measured values of each foot region j, and $\vec{F}_{tj}$ is a vector containing all the values of the foot region j from the begining of the session until a given time t. Then, the threshold value for each foot region (T_j) is given by:

$$T_j = r_j \cdot h + min(\vec{F}_{tj}) \tag{7}$$

where h is the threshold percentage, an empirical value of 5% was found to be effective ($h = 0.05$). A Mamdani fuzzy inference system [15] is used to calculate the probability of each sub-phase at any given time. The membership function $\mathcal{F}$ for each sensor j at any given time t is given by:

$$\mathcal{F}_{tj} = \frac{1}{2}\left(\tanh\left(\frac{k_j(F_{tj} - T_j)}{r_j} - 1 \right) + 1 \right) \tag{8}$$

where k_j is the gain for each foot region j, and F_{tj} the measurement output of each foot region j at a given time t during the session. Effective values for k_j were empirically tuned and were set to $k_{1,2,3} = 3$ and $k_{4,5,6} = 4$. This was done by increasing k_j of each membership function $\mathcal{F}_{tj}$ until every gait phase could be detected during level walking done by a the subject.

The rules that define each sub-phase's probability are described in Table 1, were μ_{LR}, μ_{EMS}, μ_{LMS}, μ_{TS}, μ_{PS}, μ_{ISw}, μ_{MSw}, and μ_{TSw} correspond to the occurrence likelihood for the loading response, early mid-stance, late mid-stance, terminal stance, pre-swing, initial swing, mid-swing, and terminal swing sub-phases, respectively. In the block III, the fuzzy membership value FMV is calculated for each sub-phase as follows:

$$\begin{aligned}
\mu_{LR} &= min(\mathcal{F}_{t1}, 1 - max(\mathcal{F}_{t2}, \mathcal{F}_{t3}), 1 - \mathcal{F}_{t4}, \mathcal{F}_{t6}) \\
\mu_{EMS} &= min(\mathcal{F}_{t1}, 1 - max(\mathcal{F}_{t2}, \mathcal{F}_{t3}), 1 - \mathcal{F}_{t4}, 1 - \mathcal{F}_{t6}) \\
\mu_{LMS} &= min(\mathcal{F}_{t1}, max(\mathcal{F}_{t2}, \mathcal{F}_{t3}), 1 - \mathcal{F}_{t4}, 1 - \mathcal{F}_{t6}) \\
\mu_{TS} &= min(1 - \mathcal{F}_{t1}, max(\mathcal{F}_{t2}, \mathcal{F}_{t3}), 1 - \mathcal{F}_{t4}, 1 - \mathcal{F}_{t6}) \\
\mu_{PS} &= min(\mathcal{F}_{t1}, \mathcal{F}_{t4}) \\
\mu_{ISw} &= min(1 - \mathcal{F}_{t1}, 1 - max(\mathcal{F}_{t2}, \mathcal{F}_{t3}), \mathcal{F}_{t4}) \\
\mu_{MSw} &= min(1 - \mathcal{F}_{t1}, 1 - max(\mathcal{F}_{t2}, \mathcal{F}_{t3}), 1 - \mathcal{F}_{t4}, \mathcal{F}_{t5}) \\
\mu_{TSw} &= min(1 - \mathcal{F}_{t1}, 1 - max(\mathcal{F}_{t2}, \mathcal{F}_{t3}), 1 - \mathcal{F}_{t4}, \mathcal{F}_{t6})
\end{aligned} \tag{9}$$

Finally, in the block IV, the sub-phase with the maximum FMV value is selected. By calculating the duration of each sub-phase and the duration of each step, it is possible to calculate in real time the duration percentage of

Table 1: *Fuzzy rules for gait phase detection.* $\mathcal{F}_{tj}$ *with* $j \in \{1, \ldots, 6\}$, *are the membership functions for each foot regions of both insoles.* μ_i *represents the fuzzy variable that gives the probability for each sub-phase* $i \in \{1, \ldots, 8\}$

$\mathcal{F}_{t1}$	$max(\mathcal{F}_{t2}, \mathcal{F}_{t3})$	$\mathcal{F}_{t4}$	$\mathcal{F}_{t5}$	$\mathcal{F}_{t6}$	μ_i
large	small	small	N/A	large	μ_{LR}
large	small	small	N/A	small	μ_{EMS}
large	large	small	N/A	small	μ_{LMS}
small	large	small	N/A	small	μ_{TS}
N/A	large	large	N/A	N/A	μ_{PS}
small	small	large	N/A	N/A	μ_{ISw}
small	small	small	large	N/A	μ_{MSw}
small	small	small	N/A	large	μ_{TSw}

each sub-phase with respect to the gait cycle, and the time between the gait events. At every new detection of a gait sub-phase, the average duration percentage for each sub-phase is calculated from the last five steps. The gait duration is then updated eight times per gait cycle, one time per sub-phase detected. The average duration percentage of each sub-phase is obtained after the first five steps and is then updated after each sub-phase detection.

3.3. Adaptive reference generation The adaptive reference trajectory is calculated by connecting the ankle joint angle values at the gait events defined above using a cubic spline function. For example, if the TL event is detected, a cubic spline trajectory that connects the current value of the ankle joint angle reference to the HO event ankle joint angle value is calculated. The duration of the cubic spline is defined by the measured gait duration. The adaptive reference of the ankle joint angular velocity and accelerations are calculated afterwards by numerically deriving the cubic spline trajectory. For the swing phase, if the TO event is detected, the cubic spline is calculated from the current ankle joint angle reference, then follows the MD key point in the middle of the path, and ends with the IC event.

4. Adaptive Proxy-based Controller

4.1. APSMC Structure The PSMC control structure proposed in [36] is depicted in Figure 5. A virtual object, referred as proxy, was used to connect a first-order sliding mode controller and a conventional PID controller. The advantage of the PSMC control structure is that a overdamping motion can be obtained to avoid large actuator torque when a large position error occurs and a relatively accurate tracking performance can be guaranteed by the inner PID controller. To further improve the robustness of the traditional PSMC with respect to disturbances from the wearer or the environment, an

adaptive tuning algorithm is introduced to tune the parameters of the inner PID controller. The whole structure of the proposed APSMC is shown in Figure 6.

The SMC controller shown in Figure 6 is designed as

$$\tau_{smc} = F\text{sgn}(e_\sigma + H\dot{e}_\sigma) \tag{10}$$

with

$$e_\sigma = \theta_d - \theta_p \tag{11}$$

where $H > 0$ and $F > 0$ denote scalar design parameters. θ_d and θ_p represent the desired ankle angle and the proxy angle, respectively.

The adaptive PID controller is designed as follows:

$$\tau_{pid} = K_i e_p + K_i \int_0^t e_p dt + K_d \dot{e}_p \tag{12}$$

with

$$e_p = \theta_p - \theta \tag{13}$$

where θ shows the real ankle angle. K_p, K_i and K_d denotes the adaptive proportional, integral and differential parameters, respectively.

By defining

$$a = \int_0^t (\theta_p - \theta) d\tau \tag{14}$$

and

$$\sigma = \theta_d - \theta + H(\dot{\theta}_d - \dot{\theta}) \tag{15}$$

then, the SMC (10) and adaptive PID (12) controllers can be re-expressed as:

$$F_{smc} = F\text{sgn}(\sigma - \dot{a} - H\ddot{a}) \tag{16}$$

and

$$F_{pid} = K_p \dot{a} + K_i a + K_d \ddot{a} \tag{17}$$

According to the analysis in [36], The dynamics of the proxy (see Figure 5) can then be modelled as follows:

$$m_p \ddot{\theta}_p = \tau_{smc} - \tau_{pid} \tag{18}$$

where m_p is the proxy mass which is set to zero. Then, we have

$$\tau_{smc} = \tau_{pid} = \tau_m \tag{19}$$

By applying the following relationship between the signum function sgn() and the saturation function $sat()$:

$$y + X = Y\text{sgn}(z - Zy) \Leftrightarrow y = -X + Y sat\left(\frac{z/Z + X}{Y}\right) \tag{20}$$

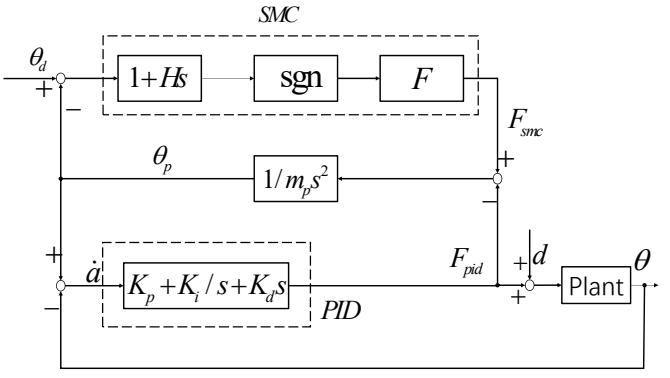

Figure 5: Structure of the conventional PSMC control

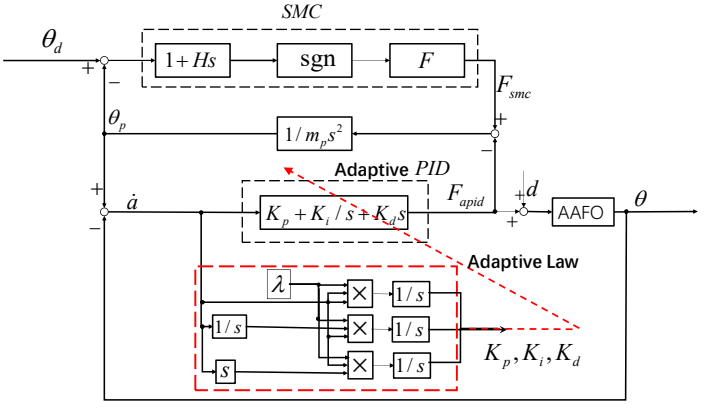

Figure 6: Structure of the proposed APSMC control

where $Y, Z > 0$ and $X, y, z \in R$.

Therefore, the whole control law can be rewritten as follows:

$$\tau_m = F sat\Big(\frac{K_d}{F}\Big(\frac{\sigma - \dot{a}}{H} + \frac{K_p\dot{a} + K_i a}{K_d}\Big)\Big) \tag{21}$$

with

$$\ddot{a} = -\frac{K_p\dot{a} + K_i a}{K_d} + \frac{F}{K_d} sat\Big(\frac{K_d}{F}\Big(\frac{\sigma - \dot{a}}{H} + \frac{K_p\dot{a} + K_i a}{K_d}\Big)\Big) \tag{22}$$

4.2. Adaptive Tuning Algorithm During walking with the assistance of the AAFO, the parameters of model (3) are different for each individual and the wearers varies their ankle joint stiffness. Moreover, the human-AAFO is subject to disturbances such as the GRF which is varying with

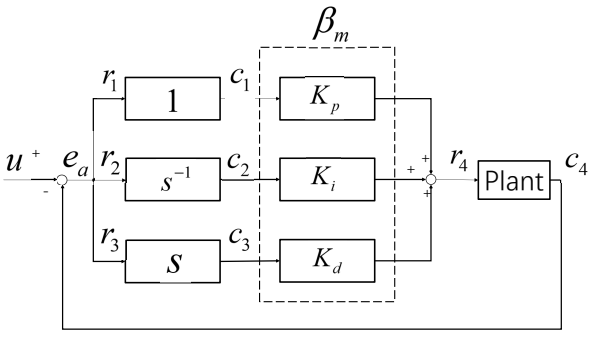

Figure 7: PID subsystem interaction.

gait phases. To deal with these issues, an on-line tuning PID controller is used. Leading up to the application of the adaptation interaction theory to the inner PID controller (see Figure 6), the inner PID based human-AAFO closed-loop system is divided into four independent subsystems such as the proportional part, integral part, derivative part and the human-AAFO system as shown in Figure 7. The PID parameters, $\beta = \{K_p\ K_i\ K_d\}$, are considered as the connection weights between subsystems. Based on the adaptive interaction theory presented in [37], the turning of the PID parameters β can be considered as a minimum problem and associated performance index $\mathcal{E}$ is designed as follows:

$$\mathcal{E} = e_a^2 = (\theta_p - c_4)^2. \tag{23}$$

where $c_4 = \theta$ shows the output of the fourth subsystem, i.e., the human-AAFO system.

According to the analysis shown in [37], $\mathcal{E}$ monotonically decreases with time, if the connection weight β is adapted as:

$$\dot{\beta} = -\gamma \frac{d\mathcal{E}}{d\beta} \tag{24}$$

with $\gamma > 0$,

Applying (24) to the on-line tuning of the PID parameters, we have:

$$\dot{\beta} = -\gamma \frac{d\mathcal{E}}{de_a} \circ G'(\tau_{pid}) \circ y_i. \tag{25}$$

where y_i, $i \in \{1, 2, 3\}$ shows the input of each subsystem as shown in Figure 7. $G'(\tau_{pid})$ represents the Frechet derivative of the human-exoskeleton system model G with input τ_{pid} and output θ.

From (17) and (25), the on-line tuning algorithm of the PID parameters is given by:

$$\begin{aligned}\dot{K}_p &= -\gamma \frac{d\mathcal{E}}{de_a} \circ G'(\tau_{pid}) \circ \dot{a} \\ \dot{K}_i &= -\gamma \frac{d\mathcal{E}}{de_a} \circ G'(\tau_{pid}) \circ a. \\ \dot{K}_d &= -\gamma \frac{d\mathcal{E}}{de_a} \circ G'(\tau_{pid}) \circ \ddot{a}\end{aligned} \tag{26}$$

According to approximation tuning method proposed in [38], the Frechet derivative for the second order system, e.g., G, can be further simplified as:

$$G'(\tau_{pid}) \circ y_i = k y_i, \tag{27}$$

where k is a constant. Thus, (26) becomes:

$$\begin{cases} \dot{K}_p = 2\gamma k e_a \dot{a} \\ \dot{K}_i = 2\gamma k e_a a \\ \dot{K}_d = 2\gamma k e_a \ddot{a} \end{cases}. \tag{28}$$

Since $e_a = \theta_p - \theta = \dot{a}$, (28) can be further rewritten as:

$$\begin{cases} \dot{K}_p = \lambda \dot{a} \dot{a} \\ \dot{K}_i = \lambda \dot{a} a \\ \dot{K}_d = \lambda \dot{a} \ddot{a} \end{cases}. \tag{29}$$

where $\lambda = 2\gamma k$.

It should be noted that using the approximation tuning method (29), $\dot{K}_p$ is always positive when the error a in not zero. Hence, the upper limit of the K_p should be limited in practice.

4.3. Stability Analysis Define the tracking error $e = \theta_d - \theta$ and the error vector as:

$$E = [e \quad E_1] \tag{30}$$

where $E_1 = [\dot{e} \ \dot{a} \ a]$. By substituting $e = \theta_d - \theta$ to (4), the error dynamics equation is obtained:

$$J\ddot{e} + B\dot{e} + Ke = -\tau + \varphi, \tag{31}$$

with

$$\varphi = J\ddot{\theta}_d + B\dot{\theta}_d + K\theta_d - d, \tag{32}$$

where $|\varphi| \leq \delta_0$ with $\delta_0 > 0$. To demonstrate the stability of the APSMC for the system (4), the following lemma is introduced.

LEMMA 1 [36]. *Considering the closed-loop system composed of system (4) and an adaptive PID controller (17) and (29) that accepts an input* $u = \dot{\theta}_p - \dot{\theta}_d$*, there exists* K_P, K_I, K_D *that allow that the function* V_p *satisfies:*

$$V_p(E_1) \geq \delta \left\| E_1 \right\|^2, \tag{33}$$

and

$$\dot{V}_p(E_1) \leq \tau u + \delta_0 \Xi E_1 - \rho_E \left\| E_1 \right\|^2 - \rho_u \left\| u \right\|^2, \tag{34}$$

where ρ_E*,* ρ_u *and* δ *are positive numbers, and* Ξ *a constraint matrix.*

According to analysis presented in [36], the Lemma 1 holds true if the PID gains are appropriately chosen, and the on-line tuning algorithm (29) is able to obtain appropriate gains for the PID controller designed for a second order nonlinear system e.g., (4), which has been proved in [39]. For more details, please refer to [36]. Based on Lemma 1, the stability of the proposed APSMC controller can be stated as:

Proposition: Considering the closed-loop system composed of system (4) and an APSMC controller, i.e., (21), (22) and (29), and the Lemma 1 holds true. Then, there exists a closed set ξ including the origin with which $E \to \xi$ is achieved as $t \to \infty$.

Proof: The proof is given in Appendix A.

5. Experimental Evaluation

5.1. Experimental Setup Figure 8 shows a paretic patient wearing the AAFO. The AAFO is driven by a DC motor (Maxion, Switzerland) with gear transmission. The maximum output torque of the AAFO is 15 Nm. The AAFO is equipped with an incremental encoder that measures the angle θ between the foot and the shank and angular velocity $\dot{\theta}$ is derived numerically. The motion range of the AAFO is from 1.171 rad (dorsiflexion) to 2.14 rad (plantar flexion). The AAFO is controlled using a myRio-1900 card (NI, USA). At the same time, two FSRM sensors (Tekscan, USA) are used to measure the GRF used for gait phase detection. The GRF data is acquired with 100 Hz and sent to a Hub as shown in Figure 8. Both the AAFO and the FSR Hub are connected to a host PC using WiFi. The control algorithm is running in labview on the host PC, in which the data from the AAFO and the FSR sensors is synchronized.

5.2. Experimental Protocol To evaluate the performance of the proposed APSMC, three experiments were carried out. The first experiment is aimed to compare the tracking performance of the proposed APSMC to that of the conventional PSMC, and the second experiment is designed to show the effectiveness of the proposed method in assisting the paretic patients during walking. Finally, the compliance of the APSMC was evaluated.

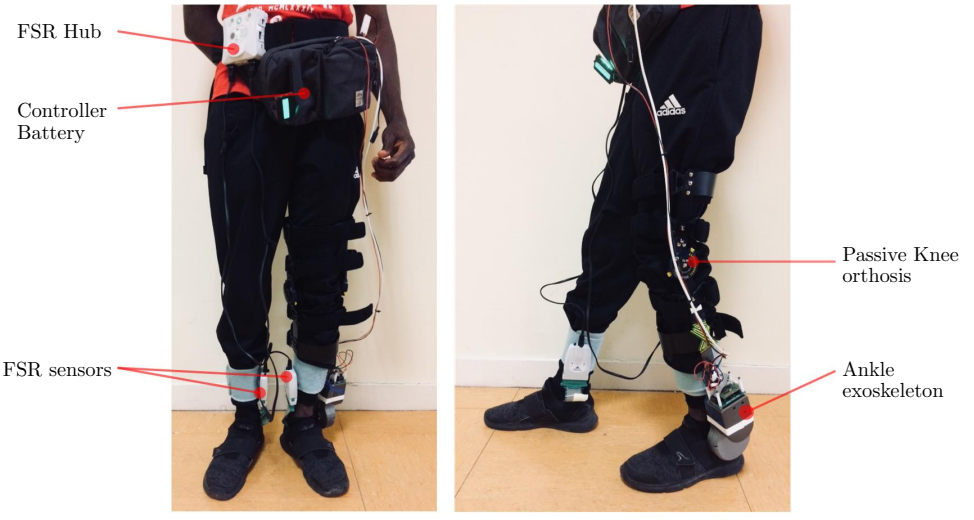

Figure 8: A paretic patient wearing the ankle joint exoskeleton and the FSR sensors

Table 2: Subjects' Information

	Subjects	Sex	Age	Height (cm)	Weight (kg)
Healthy	S_1	Male	31	180	78
	S_2	Male	31	170	76
Patient	S_3	Male	24	181	63

Two healthy subjects (see Table 2) participated in the first experiments and were asked to simulate abnormal gaits (i.e., fixing the knee joint) during walking on a treadmill with the AAFO and sensors shown in Figure 8 under three conditions: *without assistance, with PSMC control, and with APSMC control*. During each condition, the subjects were asked to walk for 80s with a low walking speed ($\approx$ 0.39m/s). The parameters for PSMC are set as $K_p = 7, K_i = 1, K_d = 0.5$, while the H is set based on the gait phases, i.e., $H = 0.01$ during swing phase and $H = 0.2$ during stance phase. The same PID control gains are also used as the initial values of the adaptive PID control gains in the APSMC, and the adaptive gain is set as $\gamma = 20$.

During the second experiment, a paretic patient (see Table 2) was asked to perform the overground walking with the AAFO with two conditions: *without assistance, and with APSMC control*. The same parameters values of the APSMC used during the first experiment were also used.

In order to evaluate the compliance of the foot-AAFO system by using the proposed APSMC controller, experiments of tracking a step input of joint angle with an amplitude of 1.8 rad were carried out when a healthy subject sat on a chair while wearing the AAFO. The step input was used to simulate the large tracking error.

5.3. Experimental Results Figure 9(a) and (d) shows respectively the generated reference angles and two healthy subjects' average ankle joint angles without assistnce. It can be observed that the simulated ankle joint angles of two subjects are significantly different from the references which are close to that of the healthy gaits as shown in [35]. Using the conventional PSMC, the subjects' ankle angles are assisted to be close to the references (see Figure 9(b) and (e)). The errors between the subjects' ankle angles and the references can be further reduced using the proposed APSMC control method. Figure 11 shows the root-mean-square-errors (RMSE) between the two subjects' ankle angles and the references during the three conditions (without assistance: Subject 1, 4.3 ± 5.6, Subject 2, 4.1 ± 5.2; with PSMC: Subject 1, 2.8 ± 4.4, Subject 2, 3.1 ± 4.0; with APSMC: Subject 1, 2.0 ± 2.9, Subject 2, 2.1 ± 2.9, unit: degrees). The tracking errors using the APSMC can be reduced by $\approx 28.6\%$ and $\approx 32.3\%$ for the two subjects compared to the ones using PSMC.

It should be noted that the references shown in Figure 9 were separately generated based on the measured group reaction forces during each condition for two subjects. Figure 10(a) presents the experimental results measured with Subject 1 using the proposed APSMC, such as the ankle angles, ankle velocities, tracking error, detected gait phases and changes of the PID gains. All phases mentioned in Section 3.1 can be clearly detected and the gait-phase based reference angles show the similar profile among different gait cycles. Regarding the performance of adaptive algorithm of the PID gains, one can observe that the tracking error during the last 30 s (RMSE: 2.01 deg) are much lower that during the first 20 s (RMSE: 4.01 deg) [see figure 10(a)]. Correspondingly, significant changes can be observed in the three PID gains in the first 20 s. As analyzed in Section 4.2, the proportional gain K_p always increase unless the tracking error converge to zero, which is difficult to be guaranteed in practice. Hence, an upper limitation is used as shown in Figure 10(b).

Figure 12 shows the average ankle angles measured with a paretic patient during two conditions: without assistance and with APSMC. The ankle joint trajectory, velocity, and detected gait phases when the patient was assisted using APSMC method are presented in Figure 13(a), and the changes of the PID gains in Figure 13(b). Although some abnormal gait-phase sequences were performed by the patient during some steps (see Figure 13(a)), the generated ankle references are not affected.

Some important kinematic features, such as the average range of motions (ROMs) during push off and swing phase, the average peak plantar flexion and dorsiflexion angle during push off, and the average peak dorsiflexion ankle ankle during swing phase (see Figure 12), were analyzed and shown in Figure 14. Without power assistance, the patient could perform a limited ankle joint push-off ROM, which also leads to a high peak plantar flexion angle at the end of push-off motion. Note that the peak dorsiflexion angle before the end of push-off motion without assistance is similar to that with assistance, but a lower peak plantar flexion angle at the end of push-off motion can be observed with assistance. Hence, the patient's ankle joint push-off ROM can be significantly increased by 96.3% with assistance. Similarly, there exists a significant increase (by 130.1%) of the ankle joint swing phase ROM.

5.4. Compliance Performance To compare the performances of the propose method with those of a PID control, a trial-and-error method was used for tuning the PID parameters to: $K_p = 9, K_i = 2, K_d = 1$. To guarantee similar experimental conditions, the same values of these gains in PID control are set as the initial values of the adaptive proportional, integral and derivative gains in APSMC. The adaptive gain γ is set to 20. Three trials were performed with different values of H: $H = 0.5, 0.2, 0.1$. The ankle angle and angular velocity are shown in Figure 15. The results show that with a reasonable high value of H, the system using APSMC achieves a smooth, slow and safe tracking towards the desired value. The smaller the H, the faster the tracking speed is. With a very small H, APSMC behaves closer to the PID controller. Thus, with an appropriate value of H, the APSMC insures the compliance of the system, while PID has a relative abrupt response to a high tracking error. Although small PID gains or large K_d can also increase the damping of the close-loop system, however, this cannot ensure the accurate tracking performance when the tracking error are relatively small as discussed in Section 5.3.

6. Conclusion

This paper proposes a new APSMC for tracking control of an AAFO during walking activity.APSMC is achieved by introducing a suitable adaptation of the PID gains of the conventional PSMC. Thus APSMC is able to improve the tracking performance of the PSMC and guarantee the compliance, i.e., safety. The synchronization between the ankle joint profile reference and the gait cycle is paramount for providing appropriate assistance. For this reason, an on-line adaptive reference trajectory is also proposed as a function of the walking speed of the wearer. This adaptive reference allowes for an automatic synchronization between the wearer gait and the desired trajectory.

The tracking experiments with the online generated reference ankle joint trajectory have been carried out to prove the efficiency of the proposed method compared to the PSMC.The safety aspects of APSMC have been also evaluated by tracking experimentally a step signal input, which simulates a relative high tracking error. The experiment results show that APSMC provides better tracking performances with repsect to the standard PSMC and at the same time is safer than PID controller.

Appendix

A. Stability Analysis of the APSMC

To analyze the stability of the APSMC, a Lyapunov function candidate is chosen as:

$$V(E) = V_p(E_1) + \|F(e - \dot{a})\|_1 \tag{35}$$

Obviously, $V(E) > 0$ for any $E \neq 0$ and $V(E) = 0$ when $E = 0$. The derivative of (35) can be expressed as follows:

$$\dot{V}(E) = \dot{V}_p(E_1) + (\dot{e} - \ddot{a})F\mathrm{sgn}(e - \dot{a}) \tag{36}$$

From (34) and (36), we obtain:

$$\begin{aligned}\dot{V}(E) \leq & \tau u + \delta_0 \Xi E_1 - \rho_E \|E_1\|^2 - \rho_u \|u\|^2 \\ & + (\dot{e} - \ddot{a})F\mathrm{sgn}(e - \dot{a})\end{aligned} \tag{37}$$

By substituting (14) into (36) and using the fact $u = \dot{\theta}_p - \dot{\theta}_d = \ddot{a} - \dot{e}$, we obtain:

$$\begin{aligned}\dot{V}(E) \leq & (\ddot{a} - \dot{e})F\mathrm{sgn}(\sigma - \dot{a} - H\ddot{a}) + \delta_0 \Xi E_1 - \rho_E \|E_1\|^2 \\ & - \rho_u \|u\|^2 + (\dot{e} - \ddot{a})F\mathrm{sgn}(e - \dot{a})\end{aligned} \tag{38}$$

Considering $\sigma - \dot{a} - H\ddot{a} = e - \dot{a} + H(\dot{e} - \ddot{a})$, (37) becomes

$$\begin{aligned}\dot{V}(E) \leq & H(\dot{e} - \ddot{a})\frac{F}{H}[\mathrm{sgn}(e - \dot{a}) - \mathrm{sgn}(e - \dot{a} + H(\dot{e} - \ddot{a}))] \\ & + \delta_0 \Xi E_1 - \rho_E \|E_1\|^2 - \rho_u \|u\|^2 \\ \leq & \delta_0 \Xi \|E_1\| - \rho_E \|E_1\|^2 - \rho_u \|u\|^2\end{aligned} \tag{39}$$

Therefore, the tracking error $E \to \xi$ is satisfied as $t \to \infty$.

Note that the following relation has been used in the above equation

$$y^T X[\mathrm{sgn}(z + y) - \mathrm{sgn}(z)] \geq 0, \tag{40}$$

where $X > 0$, and $y, z \in R$.

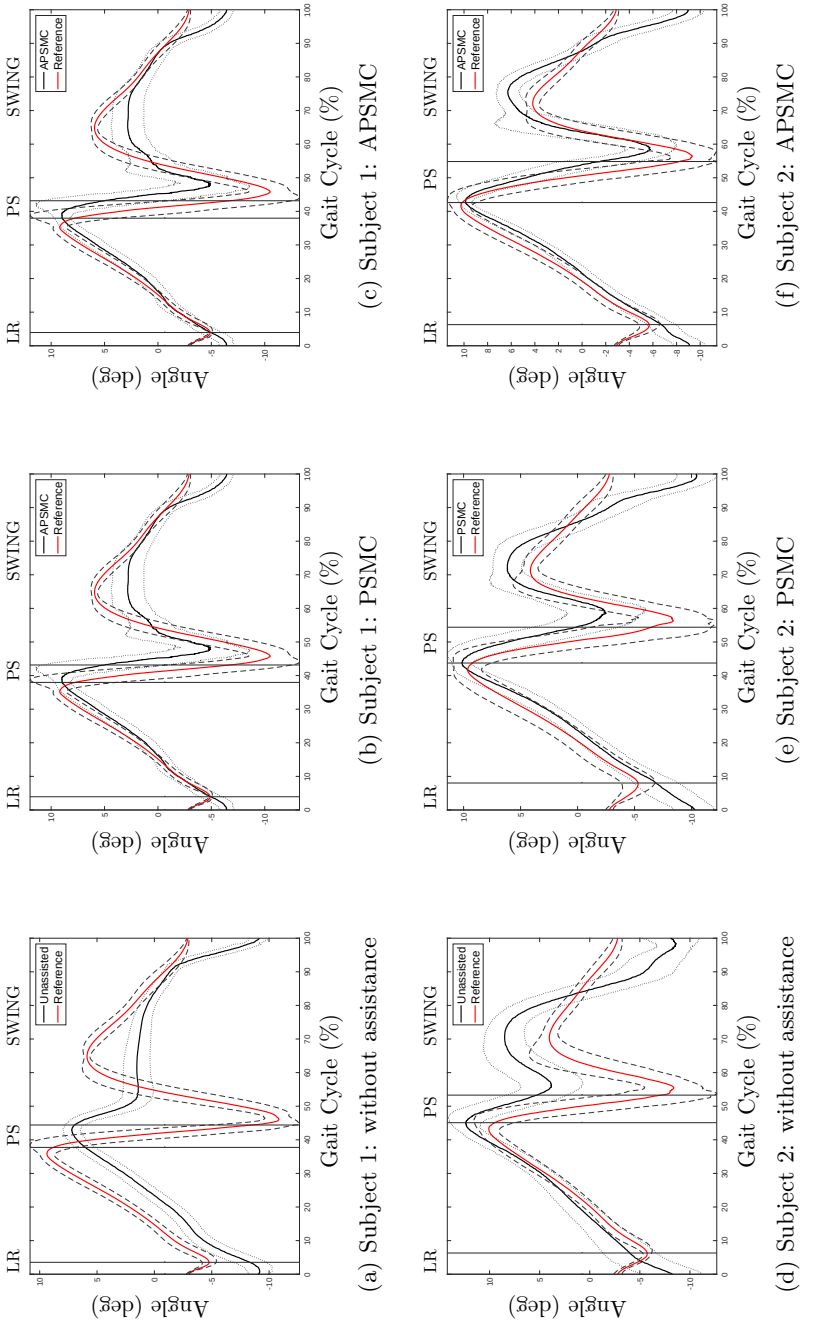

(a) Subject 1: without assistance (b) Subject 1: PSMC (c) Subject 1: APSMC

(d) Subject 2: without assistance (e) Subject 2: PSMC (f) Subject 2: APSMC

Figure 9: Average ankle joint trajectories measured under three conditions: without assistance, with PSMC control, and with APSMC control.

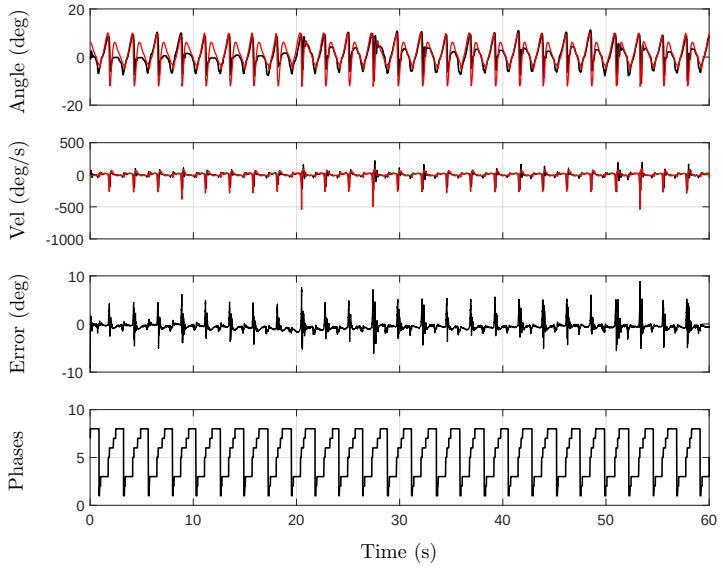

(a) The ankle angles (red line: reference; black line: measured), ankle velocities (red line: reference; black line: measured), tracking error, and detected gait phases (1:LR; 2:EMS; 3:LMS; 4:TS; 5:PS; 6:ISw; 7:MSw; 8:LSw)

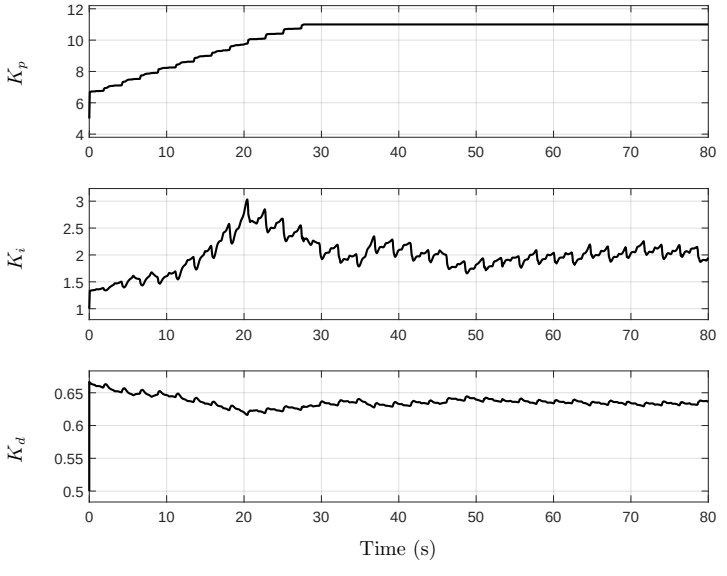

(b) The changes of the PID gains

Figure 10: Experimental results with subject 1.

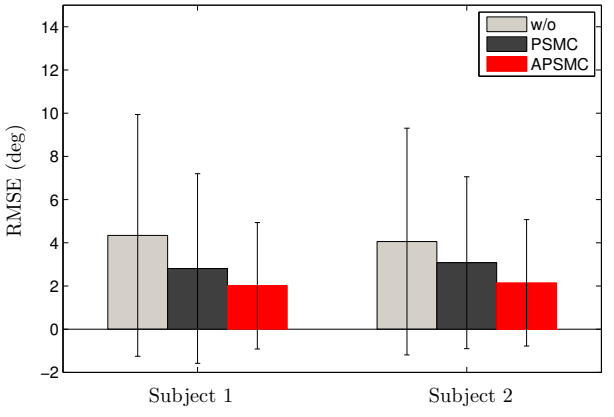

Figure 11: The measured RMSE during three conditions: without assistance (w/o), with PSMC, and with APSMC

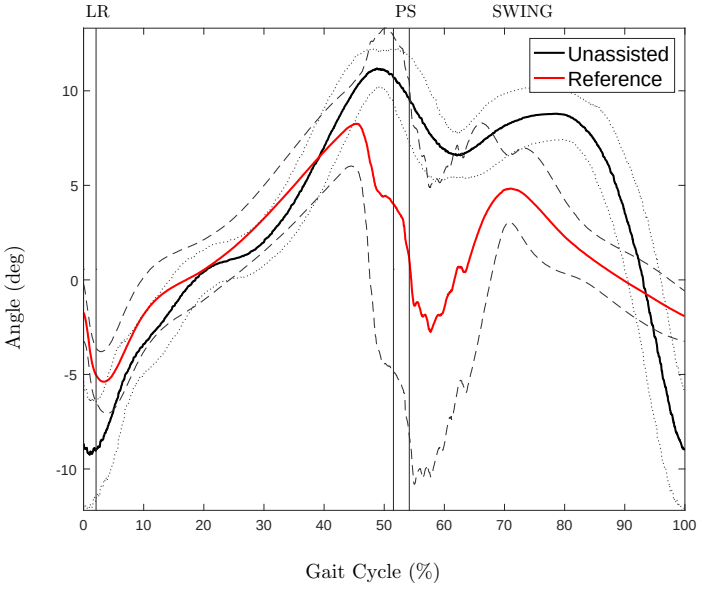

(a)

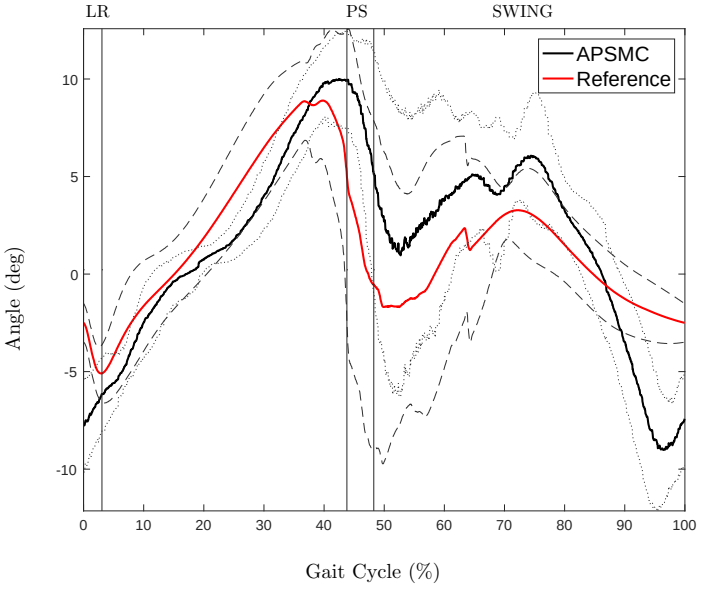

(b)

Figure 12: The patient's average ankle joint trajectories measured under two conditions: without assistance and with APSMC control. (a) without assistance; (b) with APSMC.

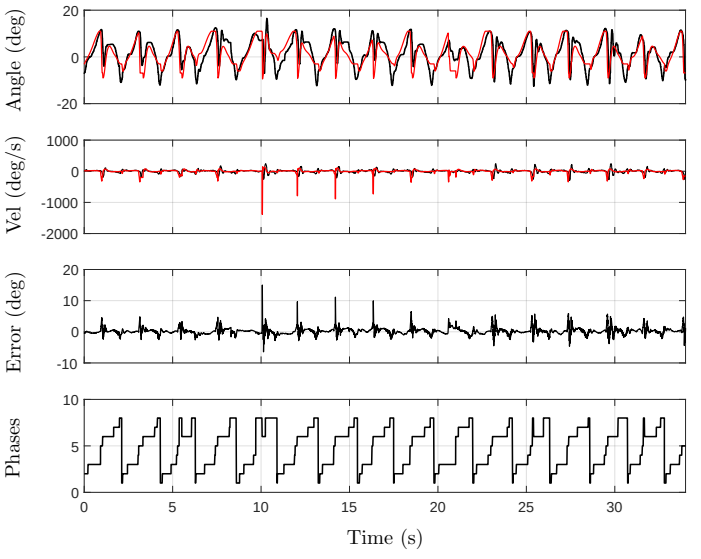

(a) The ankle angles (red line: reference; black line: measured), ankle velocities (red line: reference; black line: measured), tracking error, and detected gait phases (1:LR; 2:EMS; 3:LMS; 4:TS; 5:PS; 6:ISw; 7:MSw; 8:LSw)

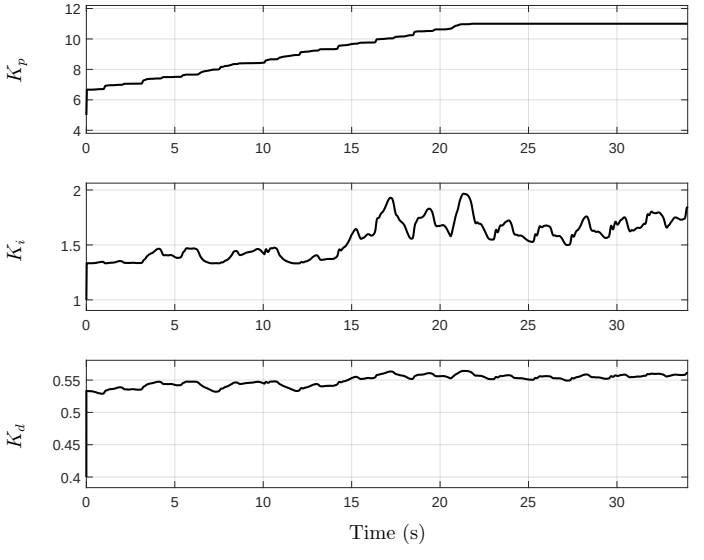

(b) The changes of the PID gains

Figure 13: Experimental results with the paretic patient

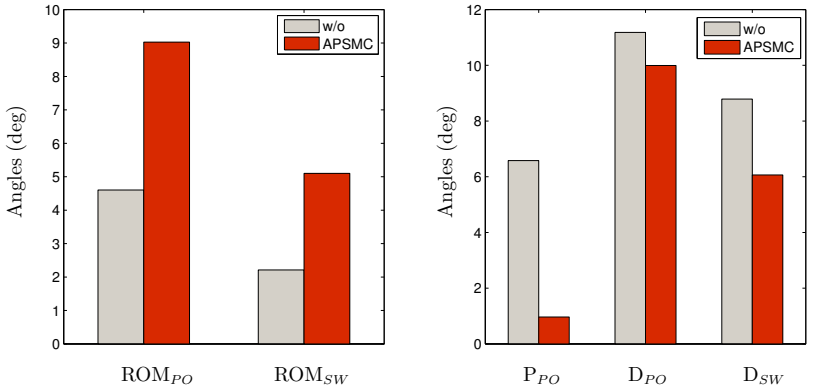

Figure 14: The changes of the main walking kinematic features of the paretic patient from the condition "without assistance (w/o)" to the condition "with assistance (APSMC). ($_{PO}$: Push off moment; $_{SW}$: Swing phase, ROM: Range of Motion, P: Planter flexion, D: Dorsiflexion)

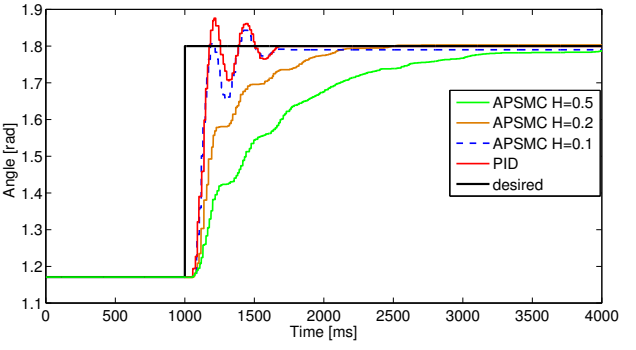

(a)

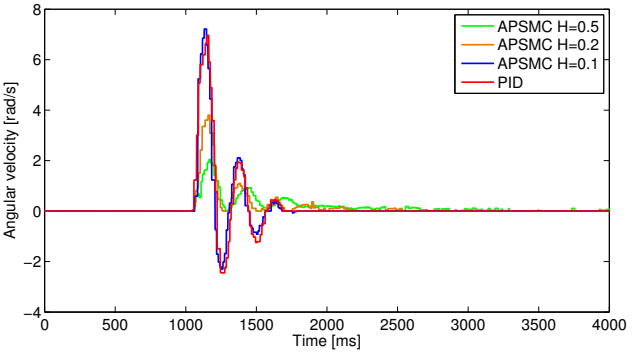

(b)

Figure 15: Safety tests using PID and APSMC. (a) Step wave tracking which simulates the big error occurs; (b) Angular velocity during the tracking process.

References

[1] JA Blaya, Dava Newman, and Hugh Herr. Active ankle foot orthoses (aafo). *Artificial Intelligence Laboratory, Massachusetts Institute of Technology, Cambridge, MA*, pages 275–277, 2002.

[2] Sungjae Hwang, Jungyoon Kim, Jinbock Yi, Kisik Tae, Kihong Ryu, and Youngho Kim. Development of an active ankle foot orthosis for the prevention of foot drop and toe drag. In *International Conference on Biomedical and Pharmaceutical Engineering (ICBPE)*, pages 418–423, 2006.

[3] Kenneth Alex Shorter, Jicheng Xia, Elizabeth T Hsiao-Wecksler, William K Durfee, and Géza F Kogler. Technologies for powered ankle-foot orthotic systems: Possibilities and challenges. *IEEE/ASME Transactions on mechatronics*, 18(1):337–347, 2013.

[4] Joaquin A Blaya and Hugh Herr. Adaptive control of a variable-impedance ankle-foot orthosis to assist drop-foot gait. *IEEE Transactions on neural systems and rehabilitation engineering*, 12(1):24–31, 2004.

[5] Joseph Hitt, A Mehmet Oymagil, Thomas Sugar, Kevin Hollander, Alex Boehler, and Jennifer Fleeger. Dynamically controlled ankle-foot orthosis (DCO) with regenerative kinetics: incrementally attaining user portability. *International Conference on Robotics and Automation (ICRA)*, pages 1541–1546, 2007.

[6] Alexander W Boehler, Kevin W Hollander, Thomas G Sugar, and Dosun Shin. Design, implementation and test results of a robust control method for a powered ankle foot orthosis (afo). *International conference on Robotics and automation (ICRA)*, pages 2025–2030, 2008.

[7] Marta Moltedo, Tomislav Baček, Kevin Langlois, Karen Junius, Bram Vanderborght, and Dirk Lefeber. Design and experimental evaluation of a lightweight, high-torque and compliant actuator for an active ankle foot orthosis. *International Conference on Rehabilitation Robotics (ICORR)*, pages 283–288, 2017.

[8] Jeffrey A Ward, Joseph Hitt, Thomas Sugar, and Kartik Bharadwaj. Dynamic pace controller for the robotic gait trainer. *International Design Engineering Technical Conferences and Computers and Information in Engineering Conference*, pages 575–581, 2006.

[9] Daniel P Ferris, Keith E Gordon, Gregory S Sawicki, and Ammanath Peethambaran. An improved powered ankle–foot orthosis using proportional myoelectric control. *Gait & posture*, 23(4):425–428, 2006.

[10] K Alex Shorter, Géza F Kogler, Eric Loth, William K Durfee, and Elizabeth T Hsiao-Wecksler. A portable powered ankle-foot orthosis for rehabilitation. *Journal of rehabilitation research and development*, 48(4):459–472, 2011.

[11] Prashant K Jamwal, Sheng Q Xie, Shahid Hussain, and John G Parsons. An adaptive wearable parallel robot for the treatment of ankle injuries. *Transactions on mechatronics*, 19(1):64–75, 2014.

[12] Yupeng Ren, Yi-Ning Wu, Chung-Yong Yang, Tao Xu, Richard Harvey, and Li-Qun Zhang. Developing a wearable ankle rehabilitation robotic device for in-bed acute stroke rehabilitation. *Transactions on neural systems and rehabilitation engineering*, 25(6):589–596, 2016.

[13] Victor Arnez-Paniagua, Hala Rifaï, Yacine Amirat, and Samer Mohammed. Adaptive control of an actuated-ankle-foot-orthosis. In *International Conference on Rehabilitation Robotics (ICORR)*, pages 1584–1589, 2017.

[14] Mohd Nor Azmi Ab Patar, Ahmad Fahmi Said, Jamaluddin Mahmud, Anwar PP Abdul Majeed, and Mohd Azraai Razman. System integration and control of dynamic ankle foot orthosis for lower limb rehabilitation. In *International Symposium on Technology Management and Emerging Technologies (ISTMET)*, pages 82–85. IEEE, 2014.

[15] Victor Arnez-Paniagua, Weiguang Huo, Ivan Colorado-Cervantes, Samer Mohammed, and Yacine Amirat. A hybrid approach towards assisting ankle joint of paretic patients. *IFES Hybrid Approaches to FES*, page 4, 2016.

[16] Juan C Pérez-Ibarra and Adriano AG Siqueira. Comparison of kinematic and EMG parameters between unassisted, fixed-and adaptive-stiffness robotic-assisted ankle movements in post-stroke subjects. *International Conference on Rehabilitation Robotics (ICORR)*, pages 461–466, 2017.

[17] Fatima el Zahraa Wehbi, Weiguang Huo, Yacine Amirat, Maher El Rafei, Mohamad Khalil, and Samer Mohammed. Active impedance control of a knee-joint orthosis during swing phase. *International Conference on Rehabilitation Robotics (ICORR)*, pages 435–440, 2017.

[18] Murray J Lawn, Makoto Takashima, Makoto Ninomiya, Jiangli Yu, Kayano Soma, and Takakazu Ishimatsu. Development of an actuation system for a rotary hydraulic brake on a low cost light weight knee-ankle-foot orthosis. *Sensors*, pages 1–4, 2015.

[19] Anindo Roy, Hermano I Krebs, Kamran Iqbal, Nathan R Macko, Richard F Macko, and Larry W Forrester. Facilitating push-off propulsion: A biomechanical model of ankle robotics assistance for plantarflexion gait training in stroke. In *International Conference on Biomedical Robotics and Biomechatronics*, pages 656–663. IEEE, 2014.

[20] Hala Rifaï, Samer Mohammed, Walid Hassani, and Yacine Amirat. Nested saturation based control of an actuated knee joint orthosis. *Mechatronics*, 23(8):1141–1149, 2013.

[21] Brahim Brahmi, Maarouf Saad, Cristobal Ochoa-Luna, and Mohammad H Rahman. Adaptive control of an exoskeleton robot with uncertainties on kinematics and dynamics. *International Conference on Rehabilitation Robotics (ICORR)*, pages 1369–1374, 2017.

[22] Mingming Zhang, Jinghui Cao, Sheng Q Xie, Guoli Zhu, Xiangfeng Zeng, Xiaolin Huang, and Qun Xu. A preliminary study on robot-assisted ankle rehabilitation for the treatment of drop foot. *Journal of Intelligent & Robotic Systems*, pages 1–9, 2017.

[23] Kartik Bharadwaj, Thomas G Sugar, James B Koeneman, and Edward J Koeneman. Design of a robotic gait trainer using spring over muscle actuators for ankle stroke rehabilitation. *Journal of biomechanical engineering*, 127(6):1009–1013, 2005.

[24] Tarek Madani, Boubaker Daachi, and Karim Djouani. Finite-time control of an actuated orthosis using fast terminal sliding mode. *International Federation of Automatic Control (IFAC)*, 47(3):4607–4612, 2014.

[25] Jeffrey Ward, Thomas Sugar, John Standeven, and Jack R Engsberg. Stroke survivor gait adaptation and performance after training on a powered ankle foot orthosis. In *International Conference on Robotics and Automation (ICRA)*, pages 211–216. IEEE, 2010.

[26] Ivanka Veneva and Nuno Ferreira. Adaptive system for control of active ankle-foot orthosis and gait analysis. In *Mathematical Methods in Engineering*, pages 153–163. Springer, 2014.

[27] Victor Arnez-Paniagua, Hala Rifaï, Yacine Amirat, and Samer Mohammed. Adaptive control of an actuated-ankle-foot-orthosis. *International Conference on Rehabilitation Robotics (ICORR)*, pages 1584–1589, 2017.

[28] R. Jiménez-Fabián and O. Verlinden. Review of control algorithms for robotic ankle systems in lower-limb orthoses, prostheses, and exoskeletons. *Medical Engineering & Physics*, 34(4):397–408, 2012.

[29] Stephen M Cain, Keith E Gordon, and Daniel P Ferris. Locomotor adaptation to

a powered ankle-foot orthosis depends on control method. *Journal of neuroengineering and rehabilitation*, 4(1):1, 2007.

[30] Michäel Van Damme, Bram Vanderborght, Bjorn Verrelst, Ronald Van Ham, Frank Daerden, and Dirk Lefeber. Proxy-based sliding mode control of a planar pneumatic manipulator. *The International Journal of Robotics Research*, 28(2):266–284, 2009.

[31] Jian Huang, Zhi-Hong Guan, Takayuki Matsuno, Toshio Fukuda, and Kosuke Sekiyama. Sliding-mode velocity control of mobile-wheeled inverted-pendulum systems. *IEEE Transactions on robotics*, 26(4):750–758, 2010.

[32] Bin Yao and Masayoshi Tomizuka. Adaptive robust control of siso nonlinear systems in a semi-strict feedback form. *Automatica*, 33(5):893–900, 1997.

[33] Ryo Kikuuwe and Hideo Fujimoto. Proxy-based sliding mode control for accurate and safe position control. In *IEEE International Conference on Robotics and Automation (ICRA)*, pages 25–30, 2006.

[34] Bader Badreddine, Alex Zaremba, Jing Sun, and Feng Lin. Active damping of engine idle speed oscillation by applying adaptive pid control. Technical report, SAE Technical Paper, 2001.

[35] Emilie Hutin, Didier Pradon, Franck Barbier, Bernard Bussel, Jean-Michel Gracies, and Nicolas Roche. Walking velocity and lower limb coordination in hemiparesis. *Gait & posture*, 36(2):205–211, 2012.

[36] Ryo Kikuuwe, Satoshi Yasukouchi, Hideo Fujimoto, and Motoji Yamamoto. Proxy-based sliding mode control: a safer extension of pid position control. *IEEE Transactions on Robotics*, 26(4):670–683, 2010.

[37] Corina Barbalata, Valerio De Carolis, Matthew W Dunnigan, Yvan Petillot, and David Lane. An adaptive controller for autonomous underwater vehicles. In *2015 IEEE/RSJ International Conference on Intelligent Robots and Systems (IROS)*, 2015.

[38] Robert D Brandt and Feng Lin. Adaptive interaction and its application to neural networks. *Information Sciences*, 121(3-4):201–215, 1999.

[39] Bader M Badreddine and Feng Lin. Adaptive pid controller for stable/unstable linear and non-linear systems. In *Proceedings of the 2001 IEEE International Conference on Control Applications (CCA)*, pages 1031–1036, 2001.

Weiguang Huo, Victor Arnez-Paniagua, Guangzheng Ding, Yacine Amirat and Samer Mohammed, Laboratoire Images, Signaux et Systèmes Intelligents (LISSI), Université Paris-Est Créteil (UPEC), 94400 Vitry-sur-Seine, France.

Email: weiguang.huo@u-pe.fr